Supplementary Information

Supplementary Figures

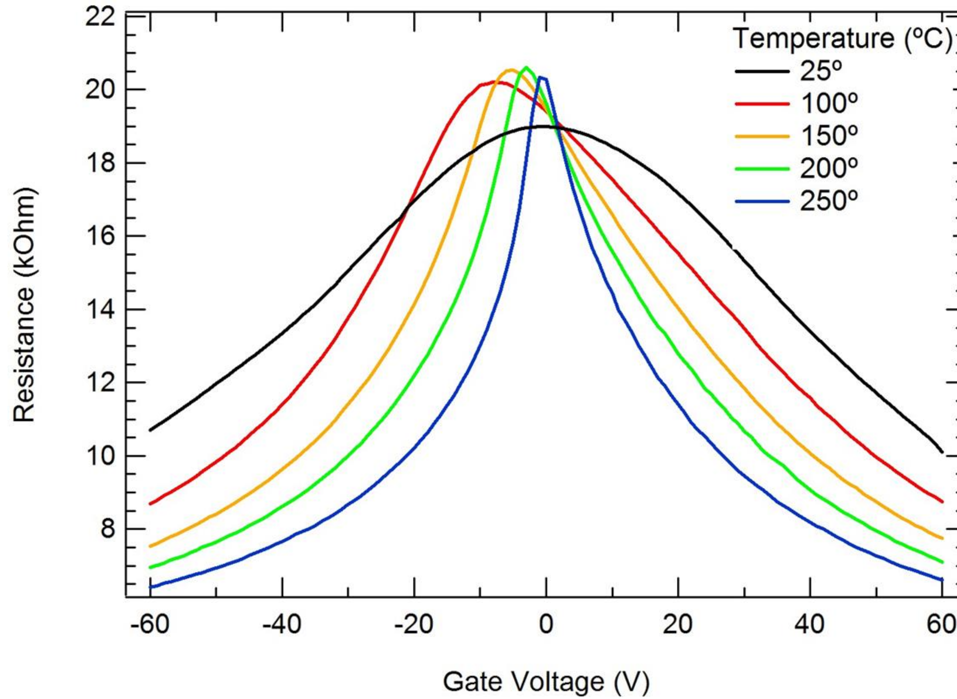

Supplementary Figure 1: Temperature-Dependent Resistance

Temperature dependence of resistance (Ohm) vs. applied gate voltage (V_G) for the graphene/ (1 um) SiN_x/(200nm)Au device studied in this work. Measurements were performed at 1 mtorr.

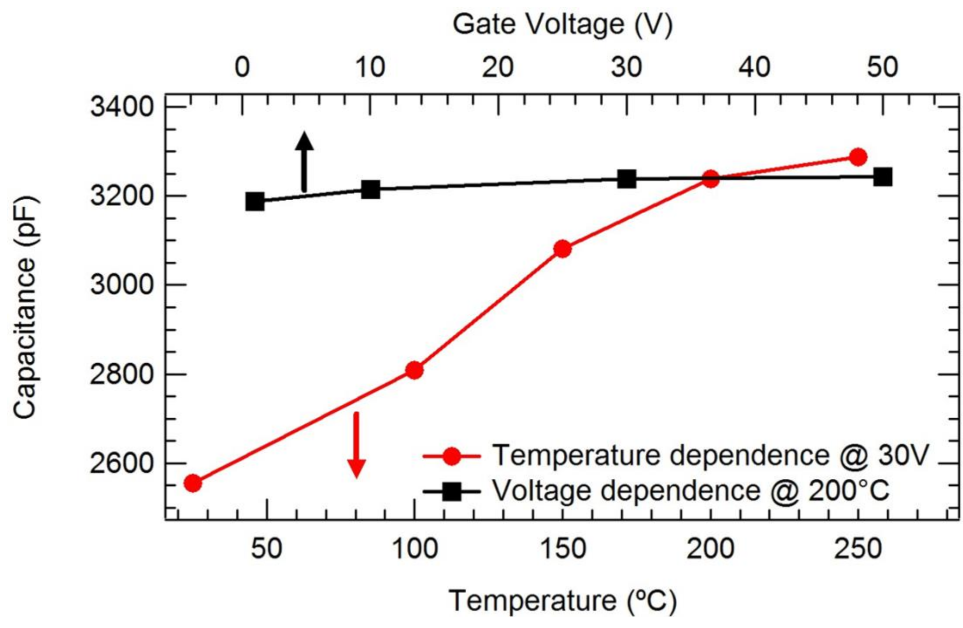

Supplementary Figure 2: Temperature- and Voltage-Dependent Capacitance

(red line) Capacitance of device as a function of temperature, taken with a 30V gate voltage. (black line) Capacitance as a function of applied gate voltage, taken at 200℃. Both measurements were taken with a 1kHz, 250mV peak-to-peak applied bias.

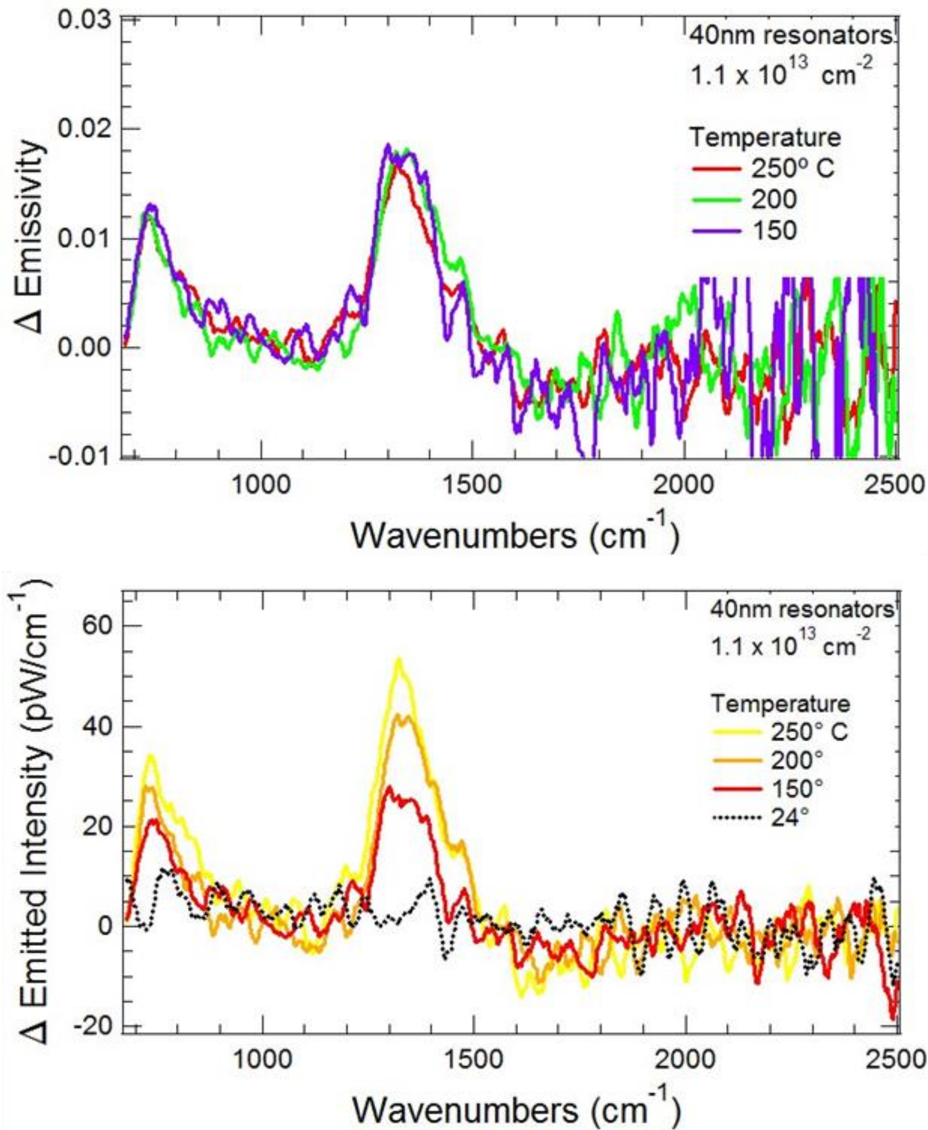

Supplementary Figure 3: Temperature Dependence of Emissivity and Emitted Intensity

Temperature dependence of change in (a) total emitted intensity and (b) emissivity for 40nm graphene nanoresonators at a carrier density of 1.1×10^{13} cm^{-2}. In order to compensate for the temperature dependent gating effects, the data at each temperature was obtained using a different applied gate voltage, such that the plasmon resonance occurred at the same frequency. The intensity of modulated thermal radiation increases as the temperature of the sample increases, but the change in emissivity displays no temperature dependence.

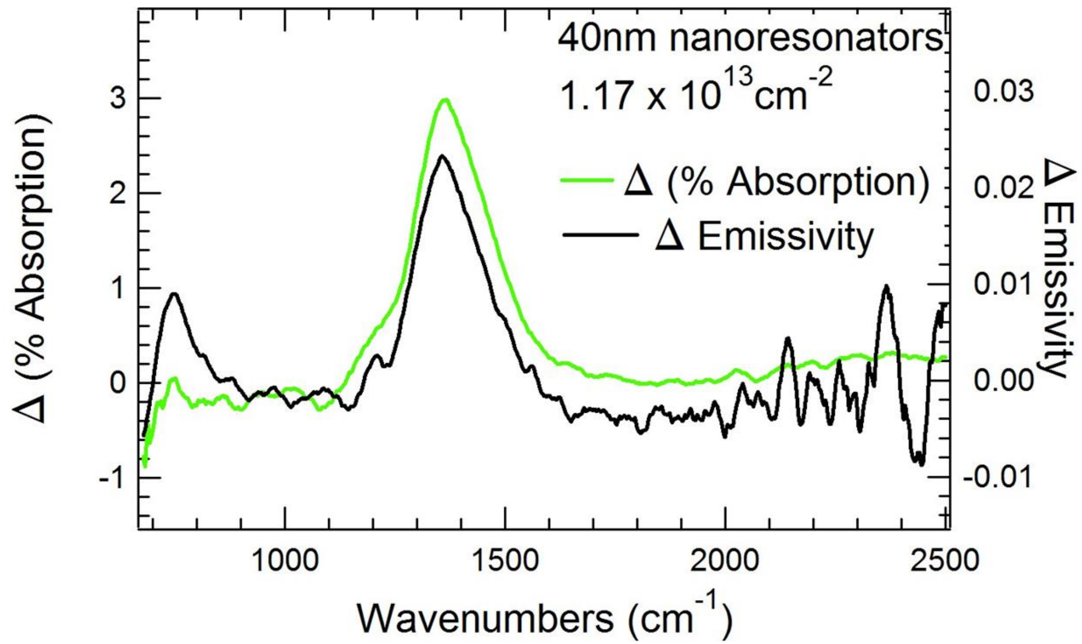

Supplementary Figure 4: Absorption and Emissivity Comparison

Comparison between carrier density dependent change in emissivity (black line) and absorption (green line) for the same device measured at comparable carrier densities.

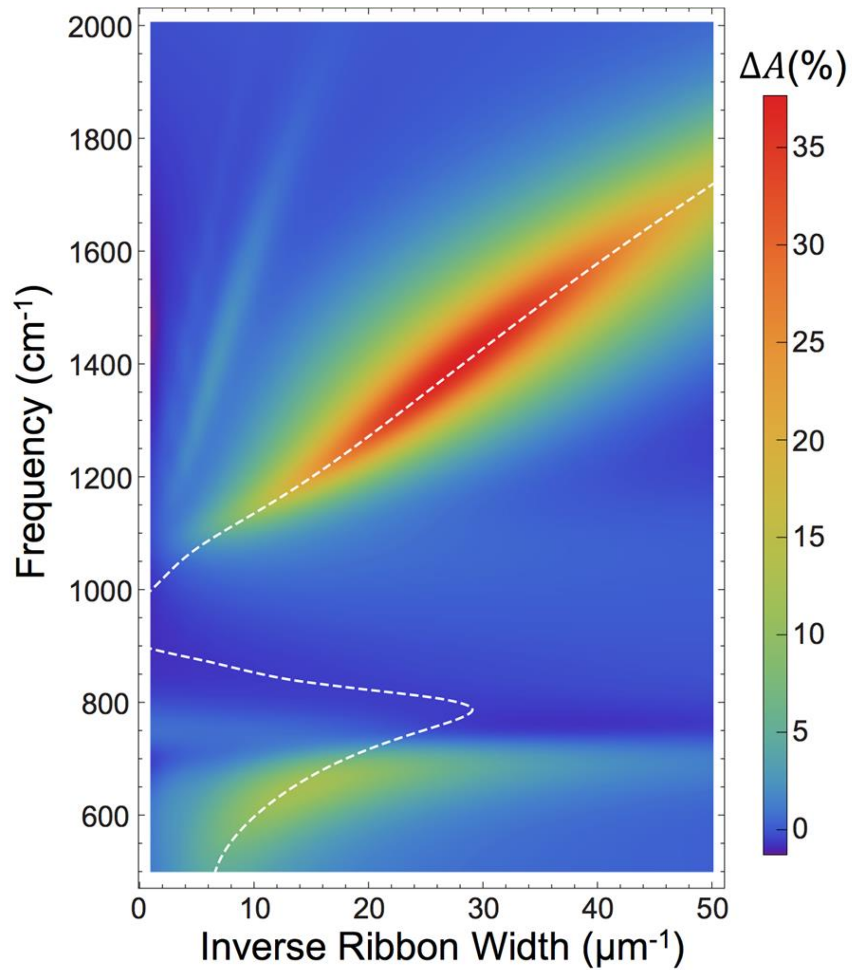

Supplementary Figure 5: Plasmon Dispersion Relation

Calculated change in absorption as carrier density is changed from zero to 1.2×10^{13} cm^{-2} for graphene nanoresonators on a 1 μm thick SiN_x membrane with a gold back reflector. The dashed white line indicates the dispersion relations for the plasmon and SPPP modes of graphene on an SiN_x substrate.[1]

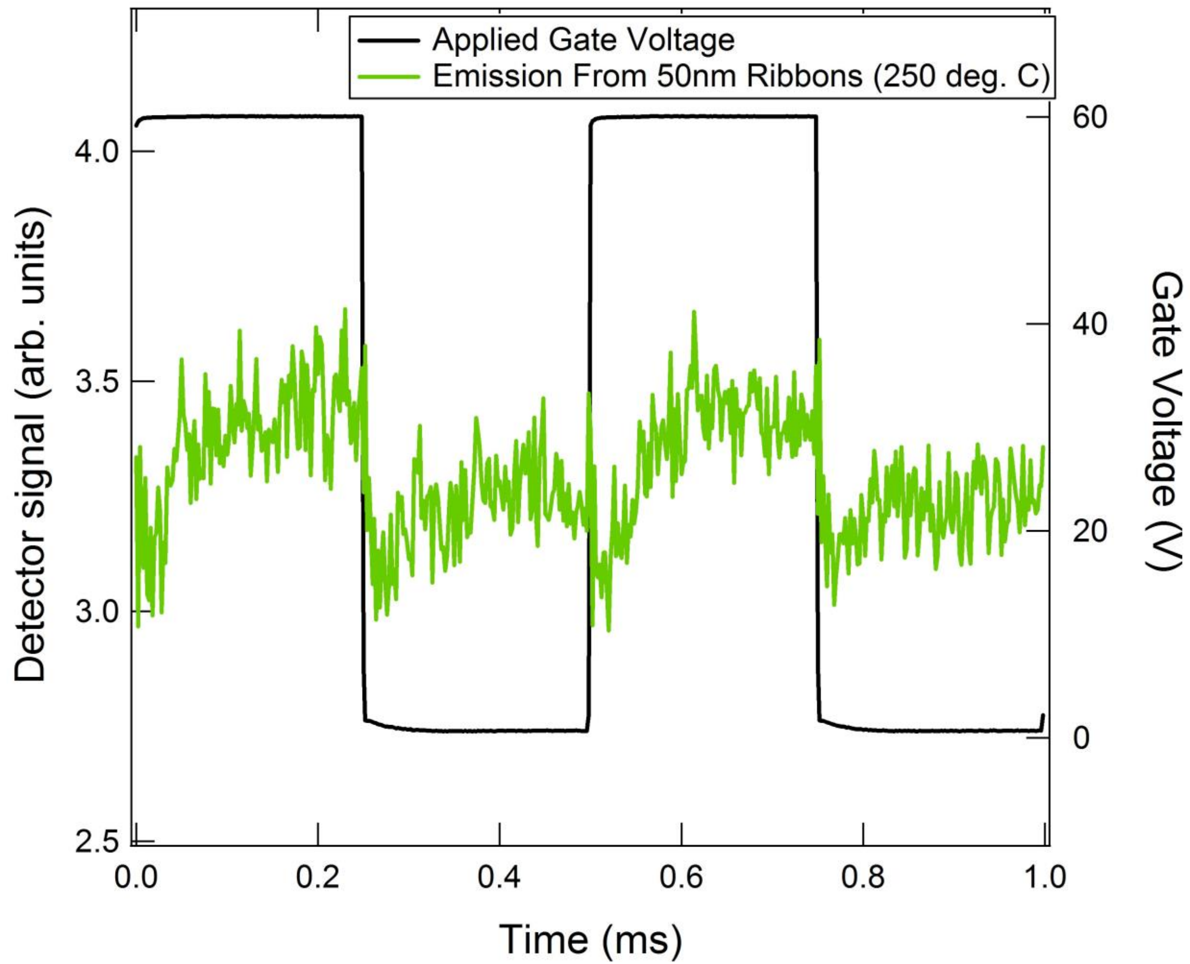

Supplementary Figure 6: kHz Modulated Signal

Temporal waveform of applied voltage signal (black line) and detector signal of emission from 50nm ribbons at 250°C (green line). A voltage of 60V corresponds to a doping level of 1.2×10^{13} cm^{-2}, resulting in a positive detector signal. A voltage of 0V corresponds to the charge neutral point of the graphene and therefore the measurement of an ‘off’ signal.

Supplementary Notes:

Supplementary Note 1. Temperature dependence of electrostatic gating

The carrier density of our device was determined by fitting the measured plasmon peak energies to the peak positions predicted using a finite element model at different carrier densities. As discovered in our previous works[2], the extracted carrier densities tended to be higher than those predicted by a simple capacitor model, and in this work we discovered that this discrepancy increased as the sample was heated. In our previous studies (performed at room temperature in atmosphere), the discrepancy was determined to be due to a combination of factors, including the unknown DC dielectric constant, κ, of the SiN_x, the effects of atmospheric impurities[3-6,] the effects of gate activated charge traps in the SiN_x[7,8], and the effect of the geometry of the device on the charge density on the surface[9]. For this study, all the above effects still apply, with the exception of the effect of atmospheric impurities, since the measurements here were performed at 1 mtorr on a sample that had been vacuum annealed. For this work, however, we must consider the temperature dependent effects on the SiN_x dielectric. In order to study those potential effects, we measured the source-drain resistance in our device as the gate voltage was varied at different temperatures. The results of those measurements are shown in Supplementary Fig. 1. As can be seen in this figure, at all temperatures the charge neutral point (CNP) occurred at low ($< |10|$ V) gate bias. This is in contrast to room temperature measurements performed in atmosphere, where the samples were found to be heavily hole doped. Additionally, it can be seen in this figure that the s-d resistance is more sharply dependent on the gate voltage at higher temperatures. We attribute this to mobile charge carriers in the SiN_x which become more mobile as the substrate is [10]. In combination with the fixed charge in the dielectric, these mobile charges add to the effective κ of the SiN_x dielectric, and they should make a large contribution at higher temperatures. In order to explore this possibility further, we performed temperature dependent $C(V)$ measurements on our device, as shown in Supplementary Fig. 2. This figure shows that, indeed, the capacitance of the device increases as the temperature as raised, with a ~30% increase in capacitance between 25° and 250° C, and a ~10% increase betwenn 150° and 250° C. For comparison, we note that a 66V gate offset at 250° C gave an equivalent carrier density as a 106V gate offset at 150° C, corresponding to a 60% increase in capacitance - larger than the change observed in our $C(V)$ measurements. We note, however, that the $C(V)$

measurements were performed at 1kHz, which may be too fast for some the mobile charges in the SiN_x. Moreover, there may also be some additional gate-activated charge traps at high temperatures that become accessible. Regardless of the precise microscopic origin, the measurements shown in Supplementary Figures 1 and 2 agree with the temperature-dependent trends we observed when fitting the carrier densities to the resonant plasmon peak positions in our device.

Supplementary Note 2. Comparison between absorption and emission

The device geometry that we use for blackbody emission measurements in this work was previously studied in terms of its gate dependent optical absorption properties.[2] In that study, it was shown that a change of up to 24.5% optical absorption could be obtained for polarized light at 1.42×10^{13} cm^{-2} carrier density. In the measurement apparatus we use here, there are a number of differences in the device properties and measurement geometry that alter these absorption properties. First, for most of the measurments performed in this work, we probed non-polarized emission. Second, in this work we could only achieve a carrier density of 1.17×10^{13} cm^{-2} due to leakage currents that occurred through the SiN_x when high gate biases were applied at high temperatures. Third, the objective used in this work had an NA of 0.65, while the previous absorption study was performed with a 0.55 NA objective. This decreases the absorption (and emissivity) of the sample due to the non-isotropic angle dependence of the nanoresonator absorptivity[11]. Fourth, the measurements here were performed through a 1 mm KBr window on the vacuum stage. This window offsets the focal plane of the microscope, and also allows for more efficient collection of high angle emitted light, while steering more low angle light into the back of the center mirror of the Cassegrain objective. Finally, the emission and absorption measurements were performed using different MCT detectors, with the detector used for emissivity measurements having a larger spectral range and larger element size, which allowed for more collection of spurious radiation that was not properly removed with the microscope aperture.

All of the above effects should act to reduce the measured absorption and emissivity changes in the sample. Thus to find a true comparison between the change in emissivity that we measure here, and the change in absorptivity of the sample, we performed absorption measurements on the same sample using

non-polarized light with the same objective, carrier density, and vacuum stage as was used for emissivity measurements (the detectors were still different). As described in our previous work, the absorption measurements were obtained by comparing the reflectivity of the graphene nanoresonators at zero and finite carrier densities to the reflectivity of a gold mirror evaporated onto the sample. The result of those measurements is shown in Supplementary Fig. 4. As can be seen in this figure, there is a strong agreement between the change in absorption to the change in emissivity, with the maximum absorption being 3.0%, and the maximum change in emissivity being 2.4%. The difference is likely due to the different detectors used for the measurements. The discrepancy at low frequencies (i.e. 730 cm^{-1}) is also due to the different detectors, as the detector used for absorption measurements had almost no sensitivity in that range.

Supplementary Note 3. Plasmonic dispersion of graphene on SiN_x

The dispersion relation for the plasmonic modes of graphene on SiN_x deviates from the expected square root dispersion for bare graphene due to graphene plasmon – SiN_x phonon coupling, which forms hybridized surface phonon plasmon polariton (SPPP) modes. The result of this coupling can be seen in Supplementary Fig. 5, where we plot the calculated dispersion relation for graphene on SiN_x, and also the inverse width dependent change in absorption (ΔA) for graphene nanoresonators as the carrier density is increased from zero to 1.2×10^{13} cm^{-2}. Simulations were performed by finite element methods within a local random phase approximation.[12] These calculations consider a scale-invariant plasmon phase shift upon edge reflection, as described in previous works[1] As can be seen in this figure, the graphene plasmon/SPPP dispersion relation displays an anti-crossing near SiN_x phonon energy, and contains three branches due to plasmon-phonon coupling. For high frequencies, the upper branch corresponds well to the energy of maximum ΔA for the graphene nanoresonators. At low frequencies, however, there is a discrepancy between the ΔA maxima and the plasmon/SPPP dispersion. As described in the text, this phenomenon is due to a destructive interference effect, which drives a large amount of absorption into the SiN_x membrane near 730cm^{-1}. As the graphene carrier density is varied, the reflection coefficient from the surface changes, which amplifies (or de-amplifies) the degree of destructive interference. Because this

process occurs at energies where the SiN_x permittivity is sharply varying, this process changes the amount of absorption into the graphene in non-trivial ways.

Supplementary Note 4. kHz Speed Signal Modulation

To test our structure as a mid-IR source at higher speeds, we performed time-resolved emission measurements on 50nm resonators at 250°C. A 2kHz modulated square wave signal was applied to the structure, with an "off" voltage of 0V, corresponding to the charge neutral point of graphene and an "on" voltage of 60V, corresponding to a graphene carrier density of 1.2×10^{13} cm^{-2}. The emission modulation was measured as a raw voltage signal from an FTIR MCTA detector using an infrared filter with transmission peaked at 1383cm^{-1} and central bandwidth of approximately 30cm^{-1}. This filter was selected to match the resonance frequency of the 50nm resonators at a doping of 1.2×10^{13} cm^{-2}, therefore isolating the plasmonic signal. The relatively small filter bandwidth results in a weakened signal and decreased signal:noise ratio. The measurement results along with the applied voltage temporal waveform are shown in Supplementary Fig. 6. A clearly modulated emission signal is seen in response to the input square wave.

In these measurements, the maximum modulation frequency was 2kHz due to limitations in the speed of the detector and the RC time constant of the combined graphene nanoresonator device, contact resistance and electrical leads. This frequency is not indicative of the inherent upper limits of the structure itself. The detector used in this experiment was optimized to match the low modulation frequency of an FTIR moving mirror, and so experienced signal decay and non-linearities outside of this frequency range. One can see in Supplementary Fig. 6 that the applied voltage signal exhibits a sharp rise time, indicating that the primary limitations here are from the detector response.

Supplementary References

1. Brar, V. W., Jang, M. S., Sherrott, M., Lopez, J. J. & Atwater, H. A. Highly Confined Tunable Mid-Infrared Plasmonics in Graphene Nanoresonators. *Nano Letters* **13**, 2541-2547, (2013).
2. Jang, M. S. *et al.* Tunable large resonant absorption in a midinfrared graphene Salisbury screen. *Physical Review B* **90**, 165409, (2014).
3. Levesque, P. L. *et al.* Probing Charge Transfer at Surfaces Using Graphene Transistors. *Nano Letters* **11**, 132-137, (2010).
4. Ryu, S. *et al.* Atmospheric Oxygen Binding and Hole Doping in Deformed Graphene on a SiO2 Substrate. *Nano Letters* **10**, 4944-4951, (2010).
5. Wang, H., Wu, Y., Cong, C., Shang, J. & Yu, T. Hysteresis of Electronic Transport in Graphene Transistors. *ACS Nano* **4**, 7221-7228, (2010).
6. Xu, H., Chen, Y., Zhang, J. & Zhang, H. Investigating the Mechanism of Hysteresis Effect in Graphene Electrical Field Device Fabricated on SiO2 Substrates using Raman Spectroscopy. *Small* **8**, 2833-2840, (2012).
7. Brar, V. W. *et al.* Gate-controlled ionization and screening of cobalt adatoms on a graphene surface. *Nat Phys* **7**, 43-47, (2011).
8. Pi, K. *et al.* Electronic doping and scattering by transition metals on graphene. *Physical Review B* **80**, 075406, (2009).
9. Thongrattanasiri, S., Silveiro, I. & de Abajo, F. J. G. Plasmons in electrostatically doped graphene. *Appl Phys Lett* **100**, (2012).
10. Dogan, A. *The Reliability of the Silicon Nitride Dielectric in Capacitive MEMS Switches* M.Sc. thesis, The Pennsylvania State University, (2005).
11. Thongrattanasiri, S., Koppens, F. H. L. & García de Abajo, F. J. Complete Optical Absorption in Periodically Patterned Graphene. *Physical Review Letters* **108**, 047401, (2012).
12. Falkovsky, L. A. & Varlamov, A. A. Space-time dispersion of graphene conductivity. *Eur. Phys. J. B* **56**, 281-284, (2007).